Journal of Rock Mechanics and Geotechnical Engineering 9 (2017) 531–542

Contents lists available at ScienceDirect

Journal of Rock Mechanics and Geotechnical Engineering

journal homepage: www.rockgeotech.org

Full Length Article

Prediction of strength and deformability of an interlocked blocky rock mass using UDEC

Y.M. Alshkane [a,b,*], A.M. Marshall [b], L.R. Stace [b]

[a] Department of Civil Engineering, University of Sulaimani, Sulaimani, Kurdistan Region, Iraq
[b] Department of Civil Engineering, University of Nottingham, University Park, Nottingham, NG7 2RD, UK

ARTICLE INFO

Article history:
Received 21 July 2016
Received in revised form
3 November 2016
Accepted 5 January 2017
Available online 4 May 2017

Keywords:
Strength
Deformability
Rock mass
Universal distinct element code (UDEC)

ABSTRACT

The accurate prediction of strength and deformability characteristics of rock mass is a challenging issue. In practice, properties of a rock mass are often estimated from available empirical relationships based on the uniaxial compressive strength (UCS). However, UCS does not always give a good indication of in situ rock mass strength and deformability. The aim of this paper is to present a methodology to predict the strength and deformability of a jointed rock mass using UDEC (universal distinct element code). In the study, the rock mass is modelled as an assemblage of deformable blocks that can yield as an intact material and/or slide along predefined joints within the rock mass. A range of numerical simulations of uniaxial and triaxial tests was conducted on rock mass samples in order to predict the equivalent mechanical properties for the rock mass under different loading directions. Finally, results are compared with the deformability parameters obtained by analytical methods.

1. Introduction

Understanding of the strength and deformability characteristics of a rock mass is critically important for the safe and economic design of many engineering systems, including dams, foundations, and excavations. Rock mass properties are essential inputs into modern design methods which routinely adopt some form of numerical modelling, for example, the finite element (FE) and finite difference (FD) methods. A range of empirical approaches has been developed to provide engineers ways of estimating the required rock mass properties. These include the rock quality designation (RQD) (Deere and Deere, 1989), the rock mass rating (RMR) (Bieniawski, 1973; Bieniawski and Orr, 1976), the tunnelling quality index (Q) (Barton et al., 1974; Barton, 2002), the geological strength index (GSI) (Hoek et al., 1995), and other equations which are based on uniaxial compression tests on jointed rock samples (Ramamurthy and Arora, 1992; Ramamurthy et al., 1993; Zhang and Einstein, 2004). These empirical methods are very useful; however, as with any empirical method, they have limitations with respect to their applicability outside the specific conditions on which they were based.

The mechanical properties of intact rock and discontinuities can be effectively determined in laboratory by triaxial and direct shear methods. However, the in situ interaction between intact rock blocks with discontinuities is very complex and it is generally not adequate to use unmodified laboratory-based measurements of rock properties within models to capture the global rock mass behaviour. Attempts to characterise large-scale rock mass properties in the laboratory are rarely undertaken due to the high cost, the difficulty in dealing with large samples, and the time required (Hoek, 1983). A range of sizes of physical models has been tested in the laboratory (e.g. 4 in × 8 in (1 in = 2.54 cm) (Brown, 1970), 60 cm × 60 cm × 130 cm (Reik and Zacas, 1978), 30 cm × 12.5 cm × 8.6 cm (Kulatilake et al., 2001), 15 cm × 15 cm × 8 cm (Singh and Singh, 2008a)), however, their ability to represent the reality of large-scale rock masses is limited since full-scale rock mass blocks cannot be effectively tested in the laboratory and block sizes have an effect on measurements of rock matrix stiffness and strength (Barton and Hansteen, 1979; Barton and Bandis, 1980; Bhasin and Høeg, 1998; Edelbro et al., 2007; Barton and Quadros, 2015). Furthermore, the effects of test configurations (e.g. platen-sample interactions) on measurements can also be significant. For example, the Hoek cell (Hoek and Franklin, 1968) has been used to study jointed rock behaviour under varying confining pressures (Asef and Reddish, 2002), however, tests in which slippage may occur along the joints should be avoided since

* Corresponding author.
E-mail address: younis.ali@univsul.edu.iq (Y.M. Alshkane).
Peer review under responsibility of Institute of Rock and Soil Mechanics, Chinese Academy of Sciences.

http://dx.doi.org/10.1016/j.jrmge.2017.01.002

the Hoek cell, which was designed to study intact rocks, can restrain jointed samples in ways that do not reflect real loading conditions (Alshkane, 2015).

Numerical modelling provides a means that can help to understand how laboratory-based measurements of rock properties relate to full-scale predictions of rock mass behaviour. The discrete element method (DEM) is a particularly attractive technique for numerically simulating the behaviour of large rock mass because of its capacity to model the intact rock blocks as well as the interactions that occur along joints. The universal distinct element code (UDEC) (Cundall, 1980; Itasca, 2011) was used to numerically model a rock mass in this work. There have been several studies involving the use of UDEC to predict the equivalent strength and deformability parameters of a jointed rock mass. The term 'equivalent' refers to parameters which could be used in analytical or continuum based models (e.g. FE or FD) to obtain results comparable to those obtained using DEM. Several authors have used this approach to study rock mass behaviour. Singh and Singh (2008b) used physical models and UDEC to investigate the lateral strain ratio in a regularly interlocked blocky rock mass under uniaxial compressive loading. They concluded that lateral strains could be attributed to the creation of voids and also permanent deformations due to slip starting along joints from the commencement of loading. Their results confirmed that the study of rock mass behaviour should be performed under appropriate levels of confining stresses. Min and Jing (2003) used UDEC to evaluate the equivalent deformability parameters of a fractured rock mass. Baghbanan (2008) predicted the equivalent strength and deformability parameters at the elastic limit because of strain-hardening behaviour after the elastic limit and concluded that it was difficult to find the ultimate or peak axial stress.

Noorian Bidgoli et al. (2013) used UDEC to predict the equivalent strength and deformability of the highly fractured rock mass model that was used by Min and Jing (2003) and Baghbanan (2008). They stated that their models did not show strain softening because they needed to stop loading when the peak strength of the models was reached so as to maintain a physical basis for an equivalent continuum assumption. However, most of their models appeared to show strain hardening and never reached peak or ultimate strength since the intact rock behaviour was assumed to be elastic.

Noorian Bidgoli and Jing (2014a) used the same fractured rock mass model (presented in Noorian Bidgoli et al. (2013)) to study the effect of loading direction on equivalent strength and deformability parameters. Their results did not show any significant effect of loading direction on the parameters but they did show that the deformation modulus increased with an increase in confining pressure. This may have been a result of the assumption of nonlinear behaviour for joint normal stiffness in their model.

The aim of this paper is to present a methodology for predicting the equivalent strength and deformability parameters of a rock mass using UDEC. The approach involves the numerical testing of rock mass samples under different confining stresses and loading directions. The paper is organised into five main sections following this Introduction. Section 2 presents a detailed description of the methodology adopted in this study. Section 3 presents a validation of the numerical model by comparing the deformation modulus for a blocky rock mass predicted by UDEC with analytical predictions. Section 4 presents the analysis of strength and deformability of a rock mass using UDEC. Finally, the paper presents conclusions in Section 5.

2. Methodology

In a UDEC analysis, the domain of interest is represented as an assemblage of rigid or deformable blocks and the contacts between the blocks are identified and updated continuously during the entire deformation process. Fig. 1 provides an illustration of the relevant joint set orientation (θ_1, θ_2) and spacing (S_1, S_2) parameters. A simple interlocked regular blocky rock mass was used in this study, as illustrated in Fig. 1b.

Individual rocks were modelled as deformable blocks with elastic-perfectly plastic constitutive behaviour using the Mohr–Coulomb failure criterion. This ensured that the UDEC analysis was able to capture any induced shear and tensile failures within the rock blocks. For joints, the area contact Coulomb-slip model (also elastic-perfectly plastic) was used.

2.1. Modelling of stress- and strain-controlled tests

Two practical ways for applying loads to intact rock or jointed rock mass samples in the laboratory are the strain (displacement) and stress (load) controlled methods (Fig. 2) (alternative methods (e.g. Pan et al., 2006; Shimizu et al., 2010) exist, however, the focus of this paper is on the more conventional strain- and stress-controlled methods). In order to determine failure load, it is often better to use strain-controlled boundary conditions (Itasca, 2011). When simulating stress-controlled tests in UDEC, as the

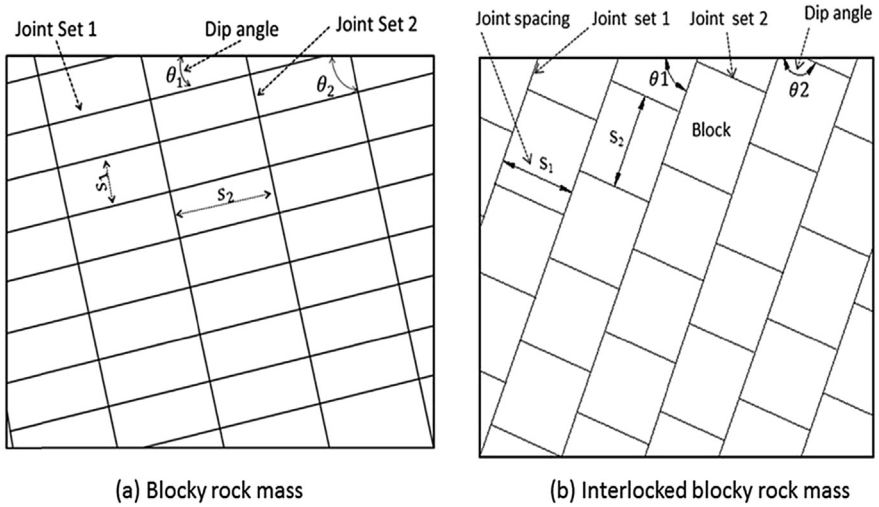

Fig. 1. Types of blocky rock masses.

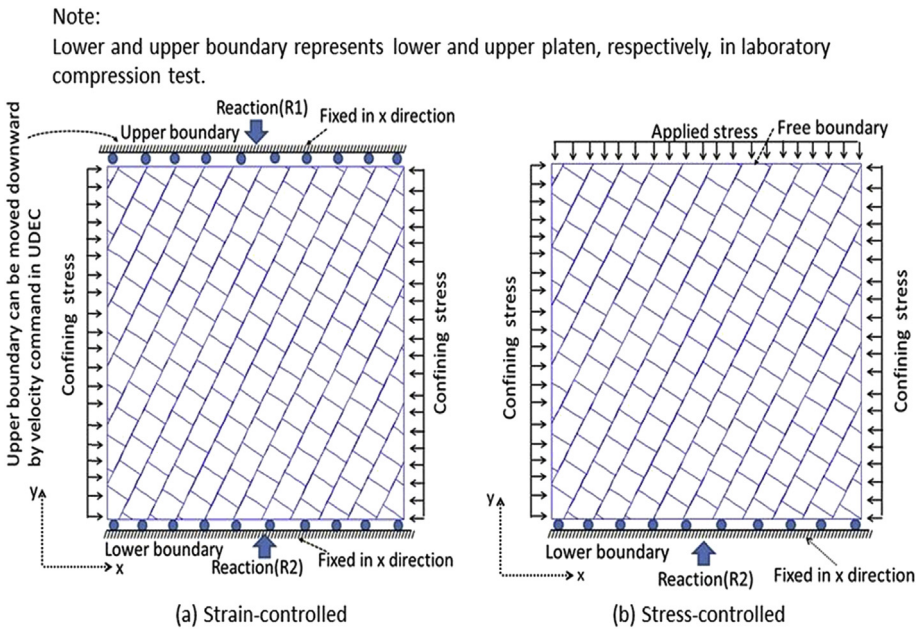

Fig. 2. Numerical simulation of laboratory compression tests on rock masses.

applied force approaches the collapse load, the system becomes difficult to be controlled (Itasca, 2011). For simulation of displacement-controlled tests in UDEC, displacements cannot be applied directly and it is necessary to fix boundaries and prescribe the velocity for a given number of steps. For instance, if the required displacement is d, a velocity ($v = d/t$) is applied for a time increment (t). Velocities should be kept small and/or increase slowly to avoid inertial "shocks" to the model which can cause problems. However, applying small velocities can be time-consuming. To address this issue, Itasca has provided a "servo-controlled" FISH (a programming language used by Itasca codes) function based on the maximum unbalanced forces in the model to reduce computational time. In this work, however, it was found that this function overestimated the axial stress after yield compared to a more rigorous (but time-consuming) methodology in which the platen movement was stopped and the model stepped to equilibrium after every 50 steps, as illustrated in Fig. 3 (velocity-controlled branch).

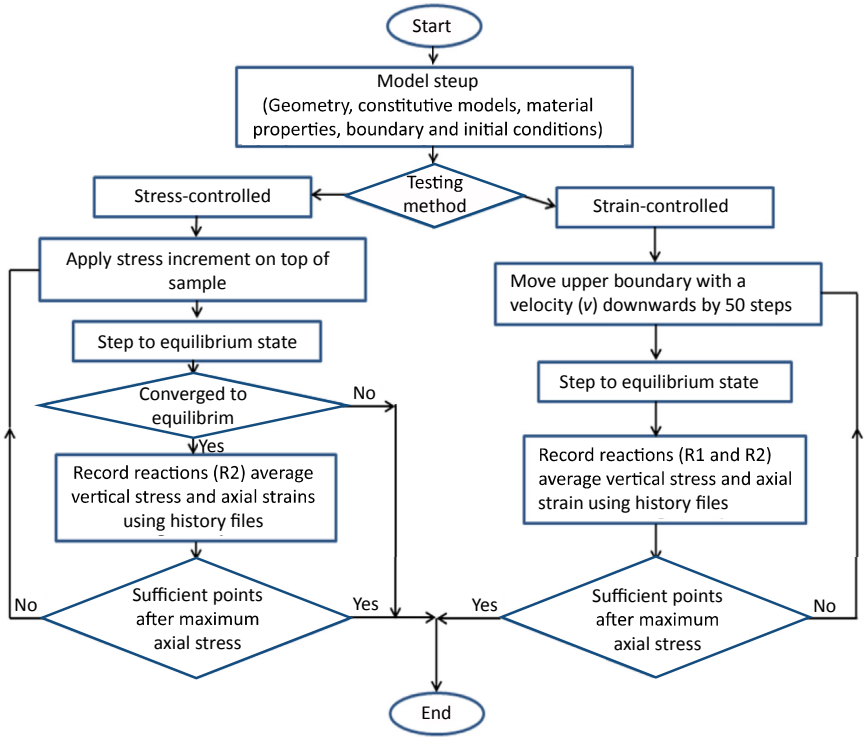

Fig. 3. Flow chart for stress- and strain-controlled UDEC analyses as illustrated in Fig. 2.

In this paper, results from UDEC simulations of stress- and strain-controlled tests on confined samples of regularly jointed rock masses are presented. A FISH function was implemented to impose the boundary conditions illustrated in Fig. 2. For the strain-controlled tests (Fig. 2a), the reactions R1 and R2 were calculated during the downward movement of the upper platen. In the stress-controlled tests (Fig. 2b), only the reaction force R2 on the lower boundary could be measured. A flow chart indicating the process of the analyses is shown in Fig. 3. The average vertical stress (σ_y) within the rock blocks was calculated for both methods in order to check that each method reached a suitable state of equilibrium before any datapoint was obtained from the model. The axial stress was computed by dividing the average value of reaction force on the platens by the sample cross-section width, and the axial strain was computed using the displacement of the top platen. In the UDEC analyses, the platens were treated as rigid boundaries because the stiffness of platens is generally much greater than that of rock samples.

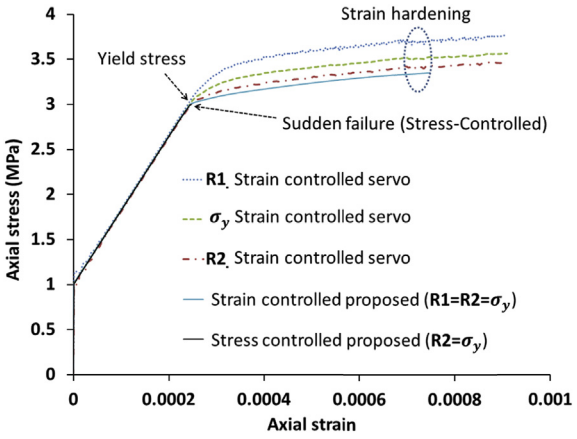

Fig. 4. Axial stress–strain results from different methods of testing a rock mass under a confining stress of 1 MPa. Note that σ_y is an average vertical stress in the block zones.

Several authors have noted a difference in results when using UDEC to replicate stress- and strain-controlled loading experiments (Noorian Bidgoli et al., 2013; Noorian Bidgoli and Jing, 2014b). It is important to note that in typical axial stress (load) controlled experiments with stiff platens, there is not a true stress-controlled (flexible) boundary on the sample-side of the platens and that the stress boundary condition is achieved by controlling the force applied to one of the platens. Therefore, a true stress-controlled boundary is not achieved on the sample-side of the stiff platen in the experiments. For experiments on blocky rock mass samples, even in stress-controlled tests, blocks adjacent to platens are restricted from rotating freely and strain hardening behaviour may be resulted in. This contrasts to a true flexible stress-controlled boundary where the blocks adjacent to the boundary are free to rotate and move, thereby allowing sliding and sudden failure. It will be shown later that numerical replication of laboratory conditions in stress- and strain-controlled loading experiments with UDEC gives similar results.

The tested rock mass consisted of two smooth joint sets, as illustrated in Figs. 1b and 2b. The first joint is continuous and the second is staggered and perpendicular to joint set 1. The samples were square in shape, similar to those presented in Noorian Bidgoli and Jing (2014a). Fig. 4 shows the axial stress–strain data for numerical samples tested under a confining stress of 1 MPa. Three methods were tested: (i) strain-control using the methodology proposed in this study (labelled 'proposed'), (ii) strain-control using the servo-controlled FISH function provided by Itasca (2011), and (iii) the stress-controlled methodology. All of the methods gave identical results of yield stress and deformation modulus (yield stress defined here as the axial stress required to fully develop slip along joint set 1). The post-yield behaviour, however, differed for the tests. The strain-controlled methods display strain-hardening behaviour after yield stress. This behaviour is a consequence of the fact that most of the joints in set 1 intersect the lower boundary of the sample, which is fixed in the vertical direction, causing the blocks to rotate after yield (illustrated in Fig. 5a and b). The axial stress using the servo-controlled method was higher than that in

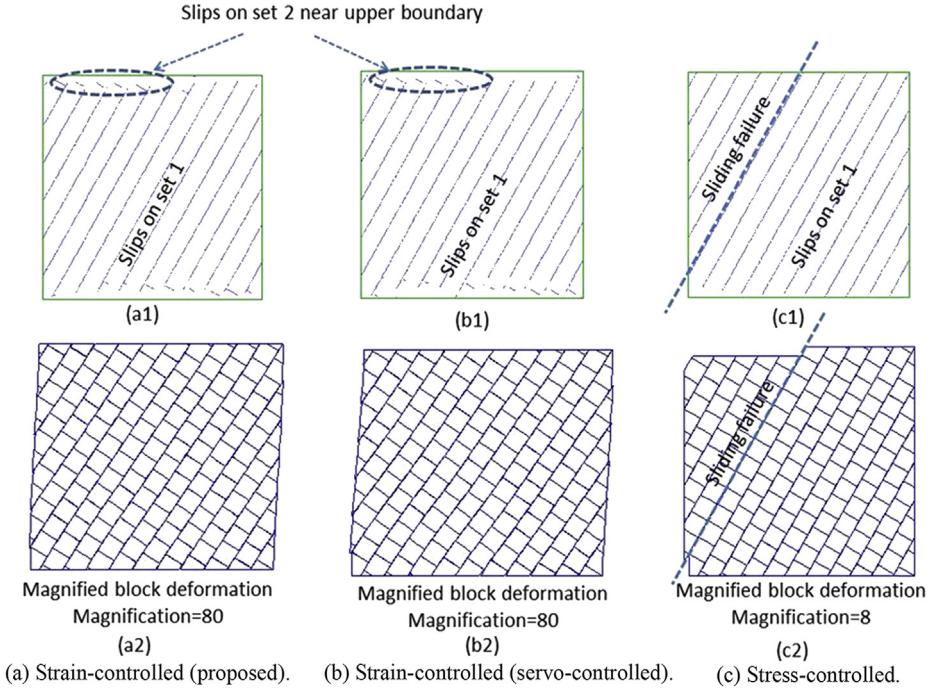

Fig. 5. Block deformations and slip along joints for different testing methods.

the proposed methodology. This is because, after yield stress, the servo-controlled system became numerically unstable. This can be illustrated by examining the unbalanced force history, as shown in Fig. 6b and c. The proposed method, which stops movement after every 50 steps and allows the model to reach equilibrium, ensures that the model is numerically stable for every datapoint obtained after yield stress. This can be seen from the history of the unbalanced force in Fig. 6c. It should be noted that the simulation time in the servo-controlled method is less than that of the proposed method. This can be overcome in the proposed method by increasing the upper platen displacement velocity, which for these tests had a minor effect on the results. Fig. 7 illustrates that the upper platen velocities between 10 mm/s and 160 mm/s produced very similar axial stress–strain results. However, the velocity should be less than 40 mm/s so as to capture the yield stress accurately.

Unlike the strain-controlled tests, the stress-controlled test did not show any strain-hardening behaviour. After yield, the stress-controlled models did not converge to a state of equilibrium, as shown in Fig. 6a. This failure mode is possible in UDEC for the stress-controlled test because the loading is applied through a flexible boundary allowing continual sliding along joint set 1, as shown in Fig. 5c.

The stress-controlled upper and lower boundary conditions illustrated in Fig. 2b are actually not representative of typical rock mass tests (e.g. the biaxial tests described in Noorian Bidgoli et al. (2013)). In these tests, the load/stress is controlled on the outer side of a stiff platen, as illustrated in Fig. 8. Some studies have indicated that when using UDEC to replicate this stress-controlled condition, results can be obtained which differ from an equivalent strain-controlled simulation (Noorian Bidgoli et al., 2013; Noorian Bidgoli and Jing, 2014b). Using the models shown in Figs. 2a and 8, results from this study indicate that the strain- and stress-controlled methods give identical results. The properties of the steel platen were taken as follows: density = 7800 kg/m^3, shear modulus = 110 GPa, and bulk modulus = 185 GPa. Fig. 9 compares the results measured by the stress-controlled tests using the setup shown in Fig. 8 with those obtained using the strain-controlled tests (note that the proposed methodology for strain-controlled test simulation was used). It can be seen that both methods give identical results under these boundary conditions.

3. Comparison with analytical results

Numerical studies should, where possible, be compared with other available predictive methods in order to develop confidence in their results. In this study, the blocky rock mass described by Barla et al. (2004) (Fig. 1a) was used to compare UDEC results with those obtained using the analytical approach of Yoshinaka and Yamabe (1986). They proposed the following equation for determination of the equivalent deformation modulus (E_{rm}) of a rock mass that consists of two continuous joint sets (as shown in Fig. 1a):

$$E_{rm} = \left[\frac{1}{E_i} + \frac{\cos^2\theta_1}{S_1}\left(\frac{\sin^2\theta_1}{k_{s1}} + \frac{\cos^2\theta_1}{k_{n1}}\right) + \frac{\cos^2\theta_2}{S_2}\left(\frac{\sin^2\theta_2}{k_{s2}} + \frac{\cos^2\theta_2}{k_{n2}}\right)\right]^{-1} \quad (1)$$

where k_s and k_n are the shear and normal stiffnesses of the joint set, respectively; S is the joint spacing; θ is the dip angle; E_i is the Young's modulus of the intact rock; and subscripts 1 and 2 denote the joint set number (see Fig. 1a). In this analytical method, the

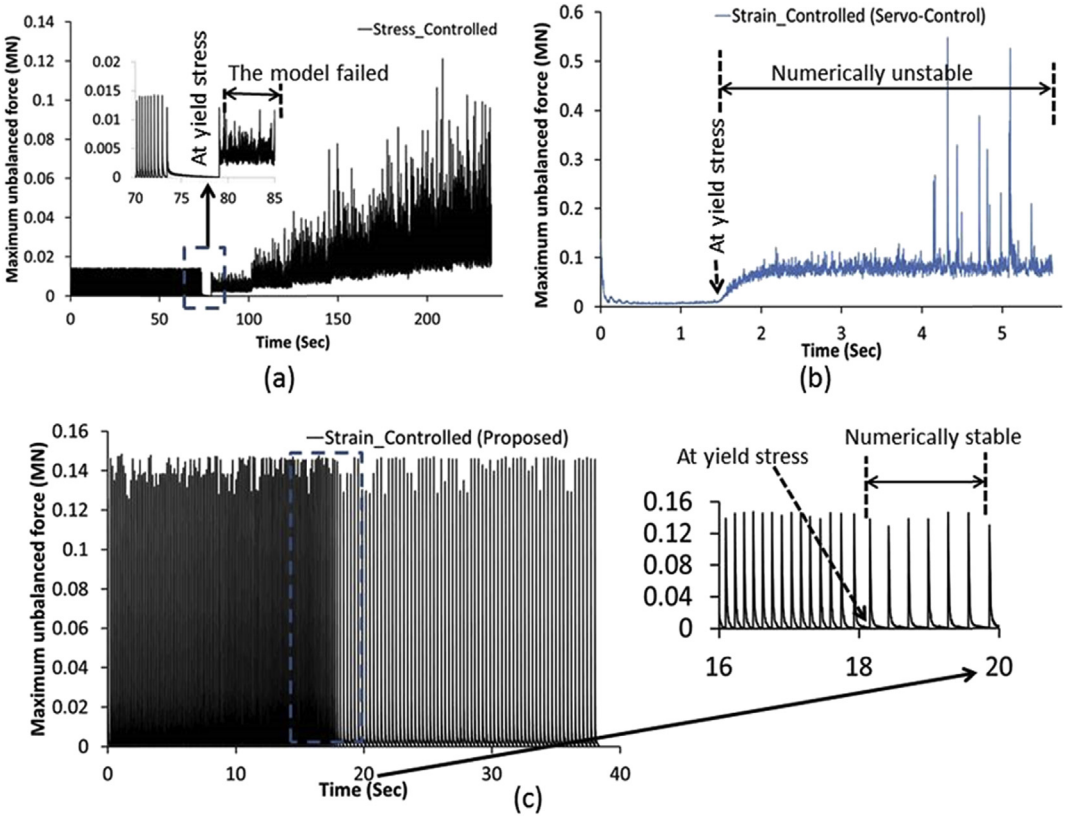

Fig. 6. Unbalanced force histories: (a) stress-controlled, (b) strain-controlled (servo-controlled), and (c) strain-controlled (proposed).

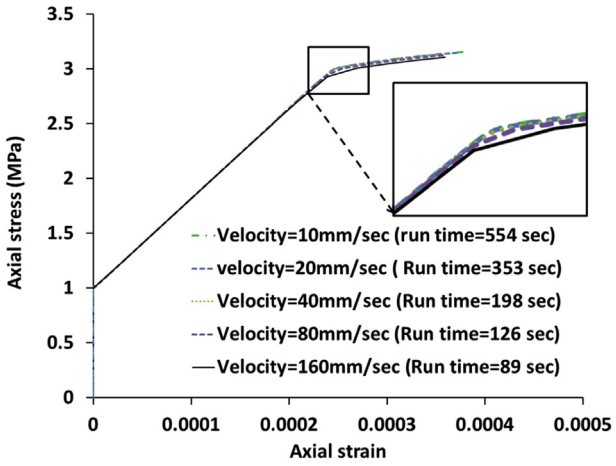

Fig. 7. Effect of applied top platen velocity on axial stress–strain results using proposed strain-controlled test method.

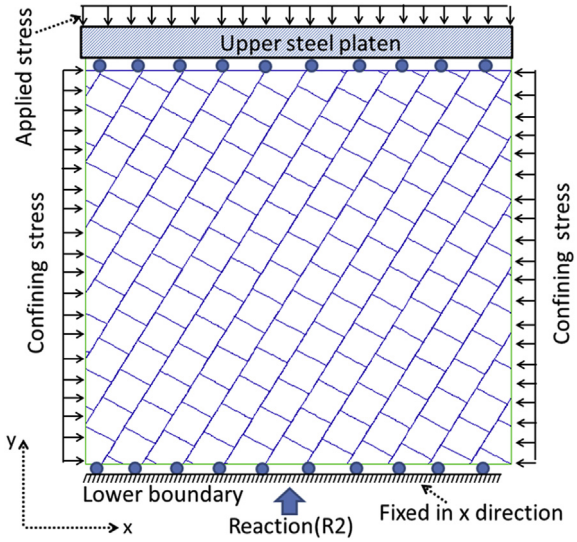

Fig. 8. Numerical sample with stress-control on outer side of upper platen.

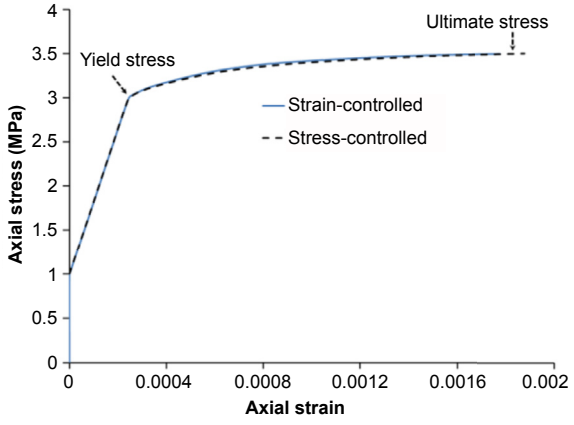

Fig. 9. Axial stress–strain data using the proposed strain-controlled method and the stress-controlled method illustrated in Fig. 8.

amount of deformation of the rock mass is related to the elastic deformation of the intact rock and joints, as well as the orientation and spacing of the joints.

The proposed strain-controlled methodology in UDEC was used to study the same blocky rock mass. The loading configuration and numerical sample are shown in Fig. 10. A rectangular sample was used with a length to width ratio of 2 in order to be consistent with typical laboratory test methods. The size of the individual blocks in the jointed rock was 2 m × 4 m. The material properties for the blocky rock mass and joint, obtained from Barla et al. (2004), are provided in Tables 1 and 2.

The rock mass was analysed numerically using UDEC by conducting large-scale uniaxial compression tests (30 m × 60 m) under a range of different directions of loading on the rock mass. The variation of loading direction was achieved by rotating two sets of joints together in anti-clockwise steps of 15°. For each step, the deformation modulus was calculated according to ISRM (1981) methods.

Fig. 11 illustrates that results from the UDEC and the analytical method agree well. The data illustrate that the deformation modulus is highly dependent on the loading direction of the jointed rock mass, with deformation modulus ranging between 2.2 GPa

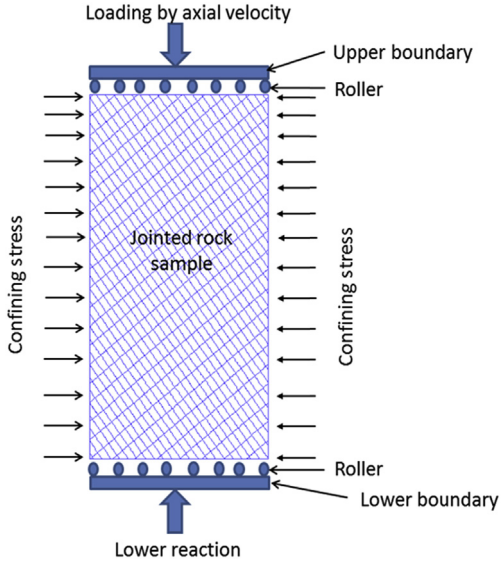

Fig. 10. Numerical sample and loading configuration for validation model.

Table 1
Material properties for blocky rock mass (Barla et al., 2004).

Material	Density, ρ (kg/m^3)	Young's modulus, E (GPa)	Poisson's ratio, ν	Cohesion, c (MPa)	Friction angle, ϕ (°)	Tensile strength, σ_t (MPa)
Intact rock	2650	20	0.3	7.5	58	3.3

Table 2
Joint properties for blocky rock mass (Barla et al., 2004).

Joints	Normal stiffness, k_n (GPa/m)	Shear stiffness, k_s (GPa/m)	Cohesion, c (MPa)	Friction angle, ϕ (°)	Tensile strength, σ_t (MPa)
Rock/rock contact	50	0.5	0	30	0

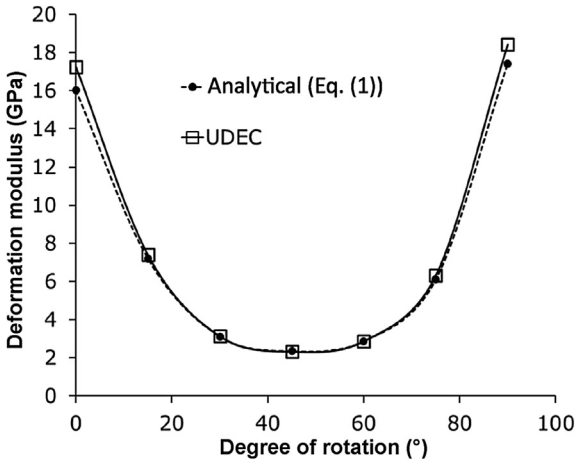

Fig. 11. Deformation modulus versus degree of rotation of blocky rock mass (validation model).

and 18.1 GPa. Note that Barla et al. (2004) adopted an equivalent deformation modulus of 10 GPa for this rock mass for the analysis of a gravity dam.

These results give confidence that the UDEC model performs as expected for this joint set condition. The advantage of the UDEC model over the analytical approach is that it can be varied to consider different joint set conditions as well as to study post-yield rock mass behaviour, as illustrated in the previous section.

4. Results and analysis

This section presents further results from a series of UDEC compression test simulations on intact rock and interlocked blocky rock mass samples in order to better understand the variation of equivalent properties with rock mass characteristics. The 'proposed' test method in Section 2 was used in all UDEC analyses. Two test cases are considered: an unconfined compression test and a confined compression test. The UDEC analyses were performed under plane strain conditions, where the out-of-plane strain is required to be zero. An objective of the work is to provide equivalent Mohr–Coulomb strength and deformability parameters, such that the results can be used within analytical and continuum-based approaches. For this reason, plane strain results were modified using the following equations (Potyondy and Cundall, 2004) in order to obtain conventional elastic parameter values:

$$\nu = \frac{\overline{\nu}}{1+\overline{\nu}} \tag{2}$$

$$E = \overline{E}\left(1-\nu^2\right) \tag{3}$$

where ν is the Poisson's ratio, $\overline{\nu}$ is the lateral strain ratio (the plane strain equivalent Poisson's ratio), E is the Young's modulus, and $\overline{E}$ is the plane strain modulus of deformation.

The understanding of rock mass behaviour is particularly relevant to the analysis of gravity dams. For this reason, the rock mass beneath the Pedrógão dam, as described by Farinha et al. (2012), was used in this analysis. The blocky rock mass in Fig. 1b is applicable to these analyses. Rock properties provided by Farinha et al. (2012) were used in this study, except for the intact rock which required additional Mohr–Coulomb parameters (not provided) because at specific joint orientations, failure may occur through intact rock blocks (Table 3 shows the properties used in this analysis). Also, for the joints, the shear stiffness was assumed to be half the normal stiffness. Table 4 shows the joint properties used in the UDEC analyses. Note that a dilation angle of zero was also used to represent smooth joints (Barton et al., 1985; Kulatilake et al., 2001).

To simulate loading conditions which may occur within a rock mass (for example, beneath a dam), the rock mass was tested using UDEC under unconfined and confined conditions at 10° intervals of joint set rotation (anti-clockwise from 0° to 90°). The ten UDEC models were named according to the dip angle of joint set 1 as follows: J0, J10, J20, …, J90. Joint set 2 was always perpendicular to joint set 1 (as shown in Fig. 1b). Tests were performed on samples sized 30 m × 60 m of both intact rock and the blocky rock mass (5 m × 5 m blocks). For the confined tests, the UDEC model was tested under a range of confining stresses from 0 to 8 MPa. The upper platen in the tests was moved downward with a velocity of 10 mm/s. The equivalent Mohr–Coulomb strength and deformability (using ISRM (1981) method) parameters were determined based on the obtained results. It should be noted that the scale effect of jointed rock mass samples on the mechanical properties of the same rock mass was studied by Alshkane (2015). It was concluded that, for a systematic jointed rock mass with fixed block size, the sample size does not have a significant effect on the axial stress–strain relationship.

4.1. Unconfined and confined compression tests

The evaluation of strength parameters using unconfined tests on rock mass samples may not provide representative values, especially when cohesionless joints are encountered in the rock mass. In some cases, the unconfined rock mass will fail under its own deadweight, as mentioned by Kulatilake et al. (2001). Fig. 12 presents the unconfined compression test results of the rock mass samples. The test produced zero unconfined compressive strength at specific joint set orientations. Also, three modes of failure are noted under low confining stress: shear mode, slip with block rotation, and sliding. The unconfined compressive strength of the rock mass is effectively zero when the dip angle of joint set 1 (θ_1) is between 30° and 80°. In these cases, the weight of the blocks is sufficient to overcome the frictional resistance to sliding along the continuous joint set 1 ($c = 0$, $\phi = 30°$).

The failure mode of sample J30 changed when it was tested under a confining stress of 1 MPa, as illustrated in Fig. 13. The failure mode changed from slip with block rotation to slip with shear and tensile failure of the intact rock blocks. Fig. 13 shows the stages of failure for model J30. At point *A*, the slope of the stress–strain response changes, and most of the staggered joints (set 2)

Table 3
Material properties for UDEC analysis.

Material	Density, ρ (kg/m^3)	Young's modulus, E (GPa)	Poisson's ratio, ν	Cohesion, c (MPa)	Friction angle, ϕ (°)	Tensile strength, σ_t (MPa)
Intact rock	2650	10	0.2	2	45	1

Table 4
Joint properties for UDEC analysis.

Joint	Normal stiffness, k_n (GPa/m)	Shear stiffness, k_s (GPa/m)	Cohesion, c (MPa)	Friction angle, ϕ (°)	Tensile strength, σ_t (MPa)
Rock/rock contact	10	0.5 k_n	0	30	0

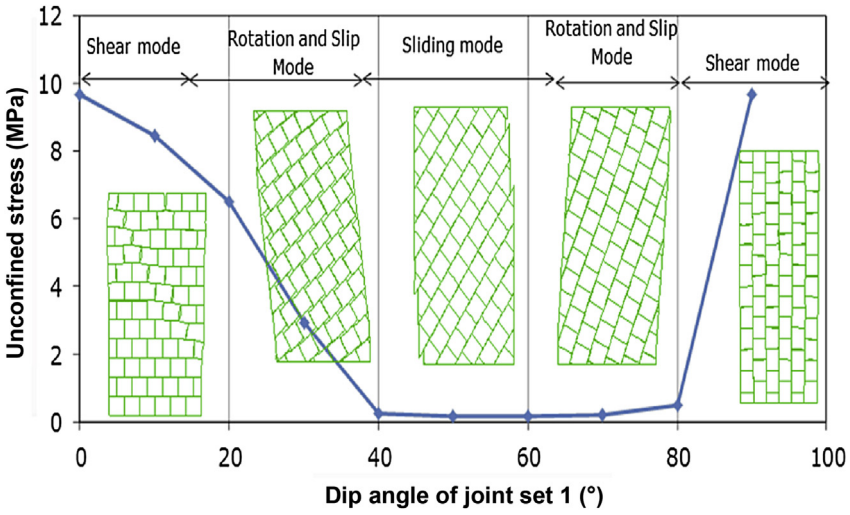

Fig. 12. Unconfined compressive strength versus joint orientation.

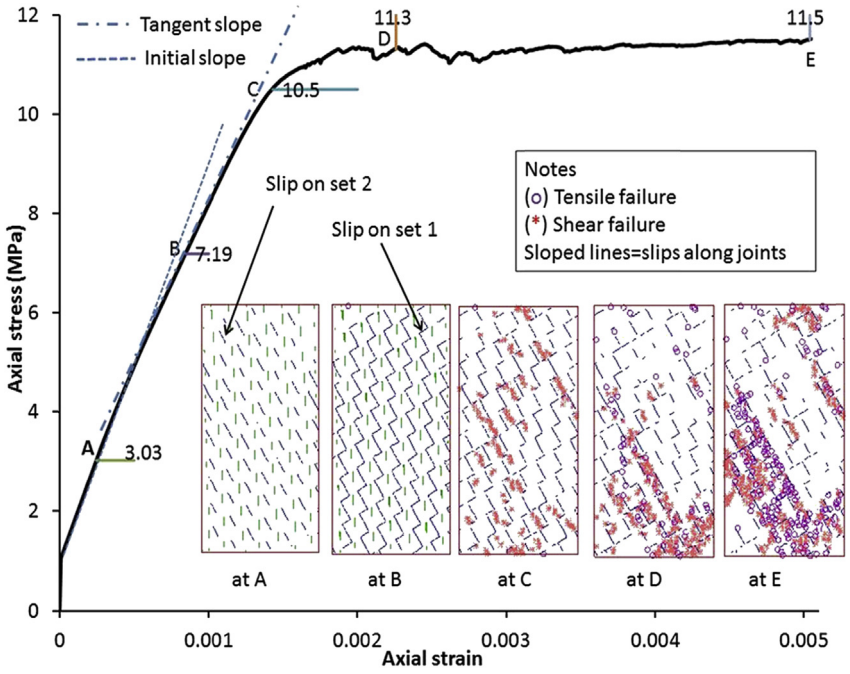

Fig. 13. Failure process for model J30 under a confining stress of 1 MPa.

have slipped. However, no slipping along joint set 1 has occurred. The curve changes from linear to nonlinear at point *B* where sliding along joint set 1 is more prominent. At this point, the discrete slippage along set 1 has still not caused a global sliding failure along the joints. The sample ultimately fails in shear at point *C* which is characterised by tensile failure within the rock blocks.

Fig. 14 shows the deformation modulus calculated for different orientations of joint set 1 for model J30 at a confining stress of 1 MPa. It was not possible to obtain the results of unconfined deformation modulus for the J30 to J80 models. Brown and Trollope (1970) had similar problems in testing physically jointed rock samples and they used small amounts of adhesive tape and a weak glue to overcome this difficulty. Numerically, a marginal confining stress (in plane strain) of 0.05 MPa was applied in order to obtain an estimate of an unconfined deformation modulus for these joint set configurations. The UDEC results are compared with empirical predictions of deformation modulus for a single set of joints orientated perpendicular to the direction of loading using the following equation (Goodman, 1989):

$$\frac{1}{E_{\mathrm{rm}}} = \frac{1}{E_{\mathrm{r}}} + \frac{1}{Sk_{\mathrm{n}}} \tag{4}$$

where E_{r} is the modulus of elasticity of intact rock. The UDEC results agree well with the empirical prediction for the relevant case of J0 and J90, however, the data illustrate that deformation modulus can vary considerably with joint dip angle, as illustrated in Fig. 12. The intact rock deformation modulus (from Table 3) is also illustrated in Fig. 14.

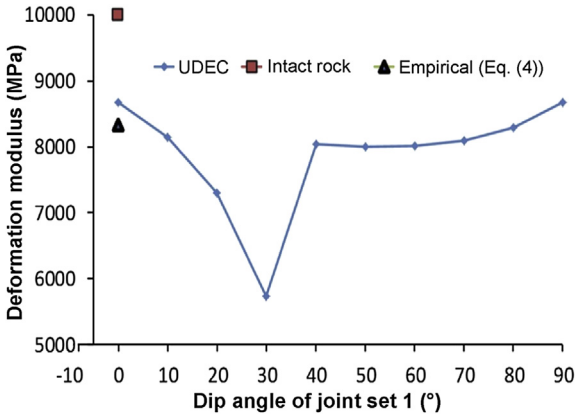

Fig. 14. Deformation modulus versus the dip angle of joint set 1 for model J30 at a confining stress of 1 MPa.

According to the unconfined test results, models J0, J30 and J60 were selected to study the effect of confining pressure on test results since these models include all the failure modes described in Fig. 12. Fig. 15 plots deviatoric stress versus axial strain for model J0 under different confining stresses. The rock mass behaviour is observed to be elastic-perfectly plastic, which indicates that the intact rock controls the behaviour of this type of rock mass. Based on the maximum axial stress values, a Mohr–Coulomb strength relationship of $\tau = 2+\sigma_n \tan 45^\circ$ is obtained.

Fig. 16a shows analysis results for model J30 and illustrates a bi-linear relationship of stress versus strain. For a confining stress of 4 MPa, the deformation modulus changes from 8.3 GPa to 7.4 GPa before the yield point, as illustrated by dashed lines in Fig. 16a. The initial modulus is due to the elastic deformation of the intact rock blocks and joints. When the joints dipping at 120° begin to slip, the deformation modulus is reduced to 7.4 GPa. Ultimately, failure occurs in the intact rock blocks and, at the same time, slipping on the joints becomes continuous. Fig. 16b shows the strength envelopes for sample J30 as well as associated Mohr–Coulomb strength relationships. The data show a bi-linear increase in strength with confining stress. The reason for this non-linearity is due to the change in failure mode that occurs as confining stress is increased; the mode changes from rotation and slip at low confining stress to shear and tensile failures of the intact rock blocks at high confining stresses. The shape of the failure envelope is similar to the bi-linear failure envelopes of saw-blade joints proposed by Patton (1966) (reported by Ladanyi and Archambault (1969)) in which sliding

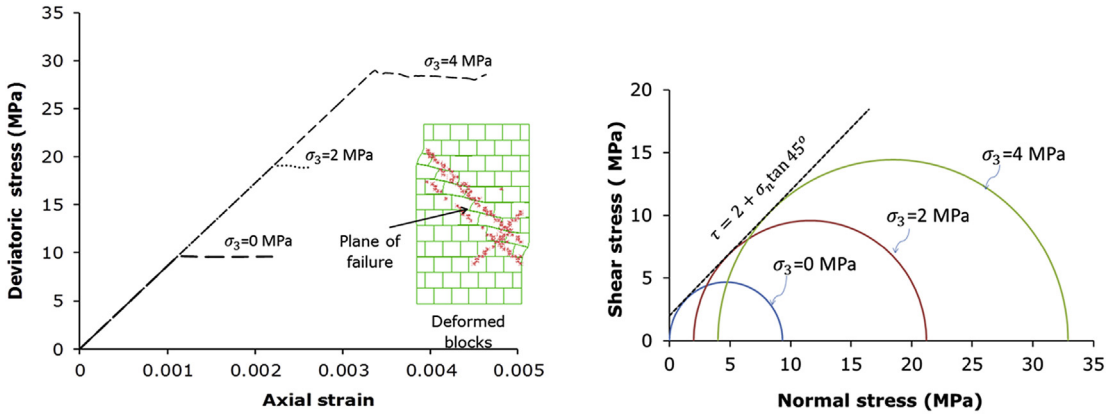

(a) Deviatoric stress-axial strain.

(b) Mohr-Coulomb strength envelopes.

Fig. 15. Effect of confining stress for model J0.

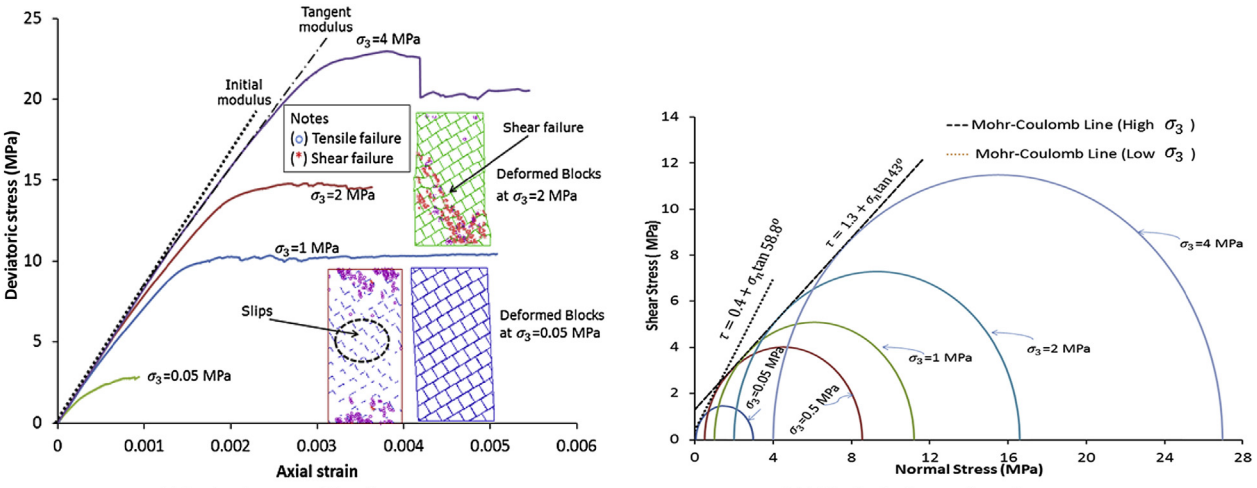

(a) Deviatoric stress-axial strain.

(b) Mohr-Coulomb strength envelopes.

Fig. 16. Effect of confining stress for model J30.

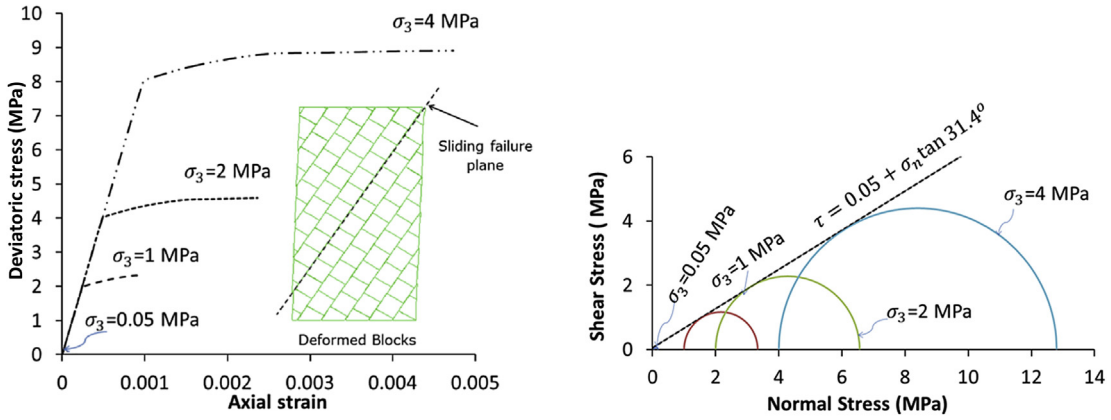

(a) Deviatoric stress-axial strain. (b) Mohr-Coulomb strength envelopes.

Fig. 17. Effect of confining stress for model J60.

occurs when there is low normal stress and failure of intact rock blocks occurs under high normal stress. Although smooth joints were used in this study, the overall behaviour is similar to Patton's model (Patton, 1966) because partial slip along the two joint sets creates a saw-blade like pattern and under high confining stress, shear failure occurs in the intact blocks. This resulting saw-blade is illustrated in the image corresponding to point *B* in Fig. 13.

Fig. 17a presents the confined compression test results for model J60, which, without confining stress, failed due to sliding along joint set 1. In this case, the joint strength controls the behaviour of the whole rock mass. The unique linear Mohr–Coulomb strength relationship $\tau = 0.05 + \sigma_n \tan 31.4^\circ$ can be obtained from the data in Fig. 17b.

The variation of calculated deformation modulus with confining stress is presented in Fig. 18. The model J30 had the lowest stiffness under low confining stress. However, when the confining stress was more than 2 MPa, all the samples showed similar values of deformation modulus and were also in general agreement with the empirical relationship (Eq. (4)).

4.2. Effect of stiffness ratio on deformability parameters

Stiffness ratio can be defined as the ratio of shear stiffness (k_s) to the normal stiffness (k_n) of the joints. Model J60 is used to demonstrate the effect of stiffness ratio on deformation modulus ($\bar{E}$) and lateral strain ratio ($\bar{\nu}$). The effect of stiffness ratio was studied in two cases with a confining stress of 1 MPa. In the first case, the stiffness ratio was increased from 0.1 to 1 while holding the normal stiffness constant at 10 GPa/m, whereas in the second case, the stiffness ratio was increased from 0.1 to 1 while keeping the shear stiffness constant at 5 GPa/m.

Fig. 19a shows that for case 1, increasing stiffness ratio results in an increase of deformation modulus and decrease of lateral strain ratio, whereas for case 2 in Fig. 19b, both deformability parameters

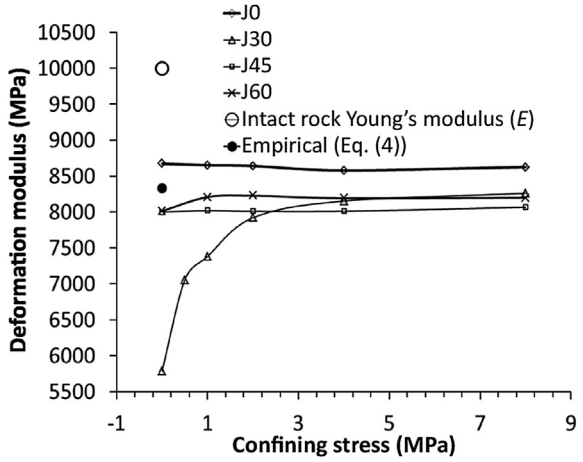

Fig. 18. Deformation modulus of selected models versus confining stress.

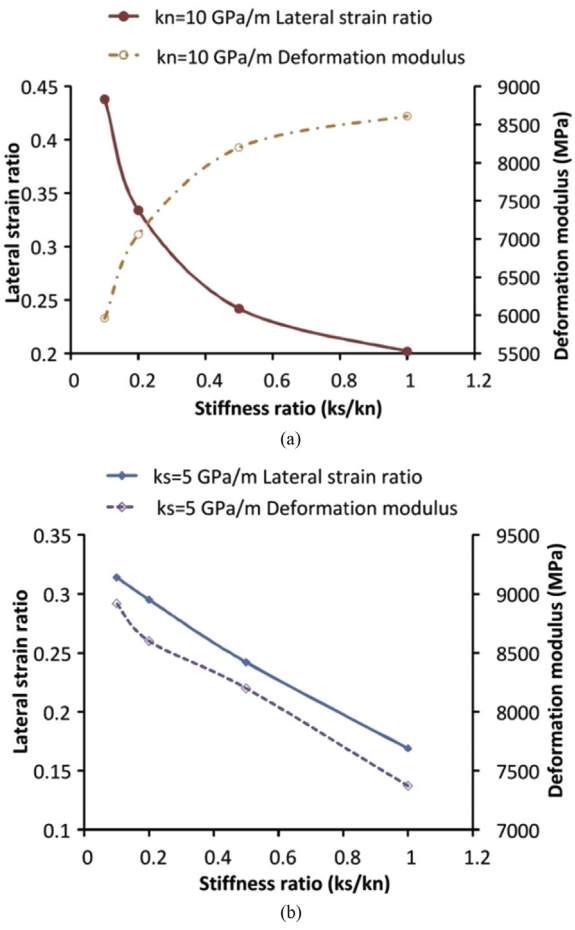

Fig. 19. Effect of stiffness ratio on deformability parameters for model J60: (a) normal stiffness constant and (b) shear stiffness constant.

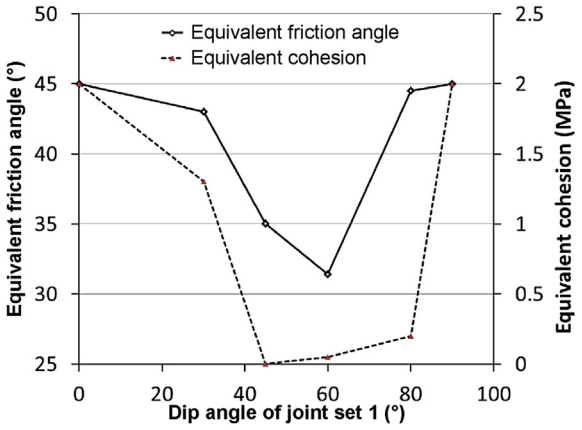

Fig. 20. Equivalent Mohr–Coulomb strength properties.

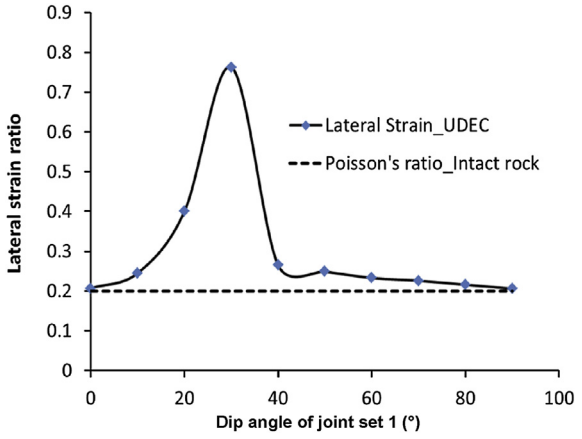

Fig. 21. Lateral strain ratio with dip angle of joint set 1.

decrease with an increase in stiffness ratio. These data illustrate the sensitivity of results to the selection of joint shear and normal stiffnesses and emphasise the importance of appropriate selection during a modelling exercise.

4.3. *Equivalent strength and deformability parameters*

The determined equivalent Mohr–Coulomb strength parameters of friction angle and cohesion intercept are summarised in Fig. 20. The deformation modulus can be obtained from Fig. 14. The lateral strain ratio was calculated for the models at 50% of the maximum compressive stress for the unconfined tests (see Fig. 21), and the Poisson's ratio can be calculated from Fig. 21 using Eq. (3). As expected, the model J30 has the maximum lateral strain ratio because it has the minimum deformation modulus under low confining stress. From these data, one can conclude that these parameters depend greatly on the loading direction on the rock masses. As can be seen from Fig. 14, the minimum deformation modulus is 5.73 GPa and the maximum one is 8.7 GPa. From Fig. 21, the range of lateral strain ratio is 0.2–0.85. These parameters should be calibrated according to Eqs. (3) and (4) because the study was achieved under plane strain condition.

5. Conclusions

In this study, methodology to predict the strength and deformability of blocky rock masses was presented. The validity of the outputs from UDEC prediction was checked against analytical solutions for a blocky rock mass. Uniaxial and triaxial tests were simulated using UDEC under plane strain conditions in order to find equivalent Mohr–Coulomb strength and deformability parameters of the rock mass. The following conclusions can be drawn:

(1) The strain- and stress-controlled test methods give identical results when simulating laboratory test boundary conditions.
(2) Strain-controlled tests using the proposed method performed better than the strain-controlled method using the servo-controlled function, especially after yield axial stress.
(3) Interlocked blocky rock masses show anisotropic behaviour.
(4) The failure mode of an interlocked blocky rock mass under low confining stress was observed to be either shear, slip and block rotation, or sliding. Under high confining stress, the slip and block rotation changed to slip with shear and tensile failure in the rock blocks.
(5) Model J30 showed a significant increase in deformation modulus with an increase in confining stress. Only this model showed a bi-linear failure envelope.
(6) Stiffness ratio (k_s/k_n) has a significant effect on the deformation modulus and the lateral strain ratio.
(7) The equivalent strength and deformability parameters significantly depend on the loading direction on the jointed rock masses.

Conflict of interest

The authors wish to confirm that there are no known conflicts of interest associated with this publication and there has been no significant financial support for this work that could have influenced its outcome.

Acknowledgements

The first author wishes to acknowledge the Ministry of Higher Education and Scientific Research in Iraq Federal for providing a full scholarship to conduct his research at the University of Nottingham.

References

Alshkane YMA. Numerical modelling investigation of rock mass behaviour under gravity dams. PhD Thesis. Nottingham, UK: University of Nottingham; 2015.
Asef MR, Reddish DJ. The impact of confining stress on the rock mass deformation modulus. Geotechnique 2002;52(4):235–41.
Baghbanan A. Scale and stress effects on hydro-mechanical properties of fractured rock masses. PhD Thesis. Stockholm, Sweden: Royal Institute of Technology (KTH); 2008.
Barla G, Bonini M, Cammarata G. Stress and seepage analyses for a gravity dam on a jointed granitic rock mass. In: Proceedings of the 1st international UDEC/3DEC Symposium: Numerical Modeling of Discrete Materials in Geotechnical Engineering, Civil Engineering, and Earth Sciences. Rotterdam: A.A. Balkema; 2004. p. 263–8.
Barton N. Some new Q-value correlations to assist in site characterisation and tunnel design. International Journal of Rock Mechanics and Mining Sciences 2002;39(2):185–216.
Barton N, Bandis S. Some effects of scale on the shear strength of joints. International Journal of Rock Mechanics and Mining Sciences & Geomechanics Abstracts 1980;17(1):69–73.
Barton N, Bandis S, Bakhtar K. Strength, deformation and conductivity coupling of rock joints. International Journal of Rock Mechanics and Mining Sciences & Geomechanics Abstracts 1985;22(3):121–40.
Barton N, Hansteen H. Very large span openings at shallow depth: deformation magnitudes from jointed models and FE analysis. In: Proceedings of the 4th Rapid Excavation and Tunnelling Conference (RETC), vol. 2. New York: American Institute of Mining, Metallurgical, and Petroleum Engineers; 1979. p. 1131–5.
Barton N, Lien R, Lunde J. Engineering classification of rock masses for the design of tunnel support. Rock Mechanics 1974;6(4):189–236.

Barton N, Quadros E. Anisotropy is everywhere, to see, to measure, and to model. Rock Mechanics and Rock Engineering 2015;48(4):1323–39.
Bhasin R, Høeg K. Numerical modelling of block size effects and influence of joint properties in multiply jointed rock. Tunnelling and Underground Space Technology 1998;13(2):181–8.
Bieniawski ZT. Engineering classification of jointed rock masses. Transactions of South African Institute of Civil Engineers 1973;15(12):335–43.
Bieniawski ZT, Orr CM. Rapid site appraisal for dam foundation by geomechanics classification. In: Transactions of the 12th Congress on large dams. Mexico City: International Commission on Large Dams; 1976. p. 483–501.
Brown ET. Strength of models of rock with intermittent joints. Journal of the Soil Mechanics and Foundations Division, ASCE 1970;96(SM6):1935–49.
Brown ET, Trollope DH. Strength of a model of jointed rock. Journal of the Soil Mechanics and Foundations Division, ASCE 1970;96(SM2):685–704.
Cundall PA. UDEC – a generalised distinct element program for modelling jointed rock. Report PACR-1–80, Contract DATA 37-79-C-0548. European Research Office and Defense Nuclear Agency, U.S. Army. 1980.
Deere DU, Deere DW. Rock quality designation (RQD) after twenty years. Contract report GL-89–1. Washington DC: U.S. Army Crops of Engineers; 1989.
Edelbro C, Sjöberg J, Nordlund E. A quantitative comparison of strength criteria for hard rock masses. Tunnelling and Underground Space Technology 2007;22(1):57–68.
Farinha MLB, Bretas EM, Lemos JV. Hydromechanical analysis for the safety assessment of a gravity dam. In: Innovative dam and levee design and construction for sustainable water management, 32nd Annual USSD Conference. New Orleans: Louisiana; 2012. p. 41.
Goodman RE. Introduction to rock mechanics. 2nd ed. John Wiley & Sons Inc.; 1989.
Hoek E. Strength of jointed rock masses. Geotechnique 1983;33(3):187–223.
Hoek E, Franklin JA. A simple triaxial cell for field or laboratory testing of rock. Transactions of the Institution of Mining and Metallurgy 1968;77:A22–6.
Hoek E, Kaiser PK, Bawden WF. Support of underground excavations in hard rock. Rotterdam: A.A. Balkema; 1995.
International Society of Rock Mechanics (ISRM). Rock characterization, testing and monitoring: ISRM suggested methods. Pergamon Press; 1981.
Itasca. UDEC (universal distinct element code). Version 5.0. Minneapolis: Itasca; 2011.
Kulatilake PHSW, Liang J, Gao H. Experimental and numerical simulations of jointed rock block strength under uniaxial loading. Journal of Engineering Mechanics 2001;127(12):1240–7.
Ladanyi B, Archambault G. Simulation of shear behavior of a jointed rock mass. In: The 11th US Symposium on Rock Mechanics (USRMS). American Rock Mechanics Association; 1969.
Min KB, Jing L. Numerical determination of the equivalent elastic compliance tensor for fractured rock masses using the distinct element method. International Journal of Rock Mechanics and Mining Sciences 2003;40(6):795–816.
Noorian Bidgoli M, Jing L. Anisotropy of strength and deformability of fractured rocks. Journal of Rock Mechanics and Geotechnical Engineering 2014a;6(2):156–64.
Noorian Bidgoli M, Jing L. Effects of loading conditions on strength and deformability of fractured rocks-a numerical study. In: Rock engineering and rock mechanics: Structures in and on rock masses, Proceedings of EUROCK 2014. CRC Press; 2014b. p. 365–8.
Noorian Bidgoli M, Zhao Z, Jing L. Numerical evaluation of strength and deformability of fractured rocks. Journal of Rock Mechanics and Geotechnical Engineering 2013;5(6):419–30.
Pan PZ, Feng XT, Hudson JA. Numerical simulations of Class I and Class II uniaxial compression curves using an elasto-plastic cellular automaton and a linear combination of stress and strain as the control method. International Journal of Rock Mechanics and Mining Sciences 2006;43(7):1109–17.
Patton FD. Multiple modes of shear failure in rock and related material. PhD Thesis. University of Illinois; 1966.
Potyondy DO, Cundall PA. A bonded-particle model for rock. International Journal of Rock Mechanics and Mining Sciences 2004;41(8):1329–64.
Ramamurthy T, Arora VK. Simple stress-strain model for jointed rocks: Proc. 7th ISRM International Congress on Rock Mechanics, Aachen, 16–20 September 1991 V1, P323–326. Publ Rotterdam: A A Balkema, 1991. International Journal of Rock Mechanics and Mining Sciences & Geomechanics Abstracts 1992;29(4):240.
Ramamurthy T, Rao GV, Singh J. Engineering behaviour of phyllites. Engineering Geology 1993;33(3):209–25.
Reik G, Zacas M. Strength and deformation characteristics of jointed media in true triaxial compression. International Journal of Rock Mechanics and Mining Sciences & Geomechanics Abstracts 1978;15(6):295–303.
Shimizu H, Koyama T, Ishida T, Chijimatsu M, Fujita T, Nakama S. Distinct element analysis for Class II behavior of rocks under uniaxial compression. International Journal of Rock Mechanics and Mining Sciences 2010;47(2):323–33.
Singh M, Singh B. High lateral strain ratio in jointed rock masses. Engineering Geology 2008b;98(3–4):75–85.
Singh M, Singh B. Laboratory and numerical modelling of a jointed rock mass. In: The 12th International Conference of International Association for Computer Methods and Advances in Geomechanics (IACMAG), Goa, India; 2008. p. 1373–80.
Yoshinaka R, Yamabe T. Joint stiffness and the deformation behaviour of discontinuous rock. International Journal of Rock Mechanics and Mining Sciences & Geomechanics Abstracts 1986;23(4):19–28.
Zhang L, Einstein HH. Using RQD to estimate the deformation modulus of rock masses. International Journal of Rock Mechanics and Mining Sciences 2004;41(2):337–41.

Dr. Y.M. Alshkane is a lecturer at the Department of Civil Engineering, College of Engineering, University of Sulaimani in Iraq. He obtained his PhD degree in Civil Engineering from the University of Nottingham in 2015. Also, he has worked for Engineering Consultancy Bureau at the University of Sulaimani since 2001. He has over 15 years of experience in teaching and geotechnical engineering, covering a variety of projects including soil investigations, soil mechanics, foundation engineering and slope engineering. His research interests cover strength and deformability of rocks using numerical and experimental methods as well as reinforcement and stabilisation of soils.

Dr. A.M. Marshall is an Associate Professor in the Faculty of Engineering at the University of Nottingham and Director of the Nottingham Centre for Geomechanics (NCG). He has worked in the field of geotechnical engineering as a researcher and consulting engineer for the past 16 years. He has authored and co-authored over 60 journal and conference papers. He completed his MASc degree at the University of Waterloo in Canada and then worked as a consulting engineer with Mott MacDonald in London, UK. Dr. Marshall was awarded his PhD from the University of Cambridge, UK, in 2009. His research focuses on physical modelling using geotechnical centrifuge testing as well as analytical and numerical modelling of geotechnical and rock mechanics problems.